IEEE 802.11ac: On Lessons Learned on OFDM MU-MIMO Transceivers with Realistic Feedback over TGac Channels with Doppler Spread

Roger Pierre Fabris Hoefel

Electrical Engineering Department
Federal University of Rio Grande do Sul (UFRGS)
Porto Alegre, RS, Brazil
roger.hoefel@ufrgs.br

Abstract-— **In this paper, we investigate the effects of channel state information (CSI) compression and feedback delay on the downlink performance of multi-user multiple input multiple output (MU-MIMO) IEEE 802.11ac systems over TGac channels with Doppler spread. We show that using degrees of freedom available at receiver side to cancel the MU interference decreases the detrimental effects of CSI imperfections on the performance of IEEE 802.11ac wireless local area networks.**

I. Introduction

The IEEE 802.11ac amendment was approved at late 2013 [1]. In one hand, the Wireless Fidelity (WiFi) semiconductor players continuous developing research and design (R&D) activities to improve the performance of second wave products, such as, implementation of downlink multi-user multiple input multiple output (DL MU-MIMO) techniques; bandwidths (BW) of *80* and *160 MHz*; four spatial streams (SS) and *256* quadrature amplitude modulation (256-QAM). This allows a maximum physical layer (PHY) throughput of *~3.5 Gbps*, while the maximum PHY throughput with 8 SS and *160 MHz* BW is *~7 Gbps* [2, pp. 213]. On the other hand, the Task Group (TG) 802.11ax was created in March 2014 to develop a new 802.11 amendment to face with the challenges of exponential increase of traffic and number of devices number in dense network scenarios and Internet of Things (IoT); competition of Long Term Evolution Unlicensed (LTE-U) to offload traffic; desire of industry to offer better user experience urged in corporative and consumer electronics market segments; pressure of chip set vendors to create a Wi-Fi market after the 802.11ac amendment [3]. Therefore, research on the effects of realistic feedback in the performance of MU-MIMO transceivers has importance in short and long terms.

The remaining of this paper is organized as follows: Section II presents our main motivations and related works. Section III briefly describes DL MU-MIMO transceiver design in 802.1ac systems. Section IV presents a consistent set of simulation results in order to investigate the effects of realistic channel state information (CSI) feedback on the system performance. Finally, our conclusions are stated in Section V.

II. Motivations And Related Work

Many papers that investigate the performance of DL MU-MIMO transceivers assume that perfect CSI information is available at both transmitter (TX) and receiver (RX) sides. For instance, it is shown in [4] that the implementation of an adaptive receiver that switches between interference whitening and interference MIMO detection allows complexity reduction with controllable performance degradation with relation to (w.r.t.) the maximum likelihood (ML) MIMO detector. However, the challenges of feedback delay and CSI compression were not fully investigated in [4]. In [5], it was carried out a performance evaluation of the DL MU-MIMO 802.11ac systems with the following channel sounding techniques: explicit (assuming compressed Givens rotation feedback); implicit (considering calibration errors). The simulation results show that a non-standardized hybrid implicit technique has a better performance w.r.t. the explicit technique specified in 802.11ac amendment [1,2]. However, the Doppler effects were not analyzed and only stations (STAs) with one antenna (i.e., low-tier devices) were assumed. In [6], the performance of 802.11ac transceivers with channel inversion (CI) and block diagonalization (BD) precoding and zero forcing (ZF) MIMO detector were studied in order to assess the performance of user selection algorithms. In [7], it was investigated the performance of generalized sphere decoding (GSD) MIMO detectors in the framework of 802.11ac DL MU-MIMO. In the references [6] and [7], the shown simulation results did not consider Doppler channels and it only showed results using compression with $(\psi,\phi)=(5,7)\,bits$ [7]] and $(7,9)\,bits$ [6,7] while in this paper we consider different levels of quantization and Doppler effects on the performance of 802.11ac systems with regularized channel inversion minimum mean squared error (RI-MMSE) precoder and interference cancellation (IC) MMSE MIMO detectors.

In this paper, we also show that the equivalent MU-MIMO channel matrix available at TX side to calculate the precoder is different from the usual mathematical model used for the DL MU-MIMO channel matrix due to the characteristics of the feedback specified in the IEEE 802.11ac amendment. A performance comparison between the 802.11ac transceivers with precoder that uses the DL MU-MIMO channel matrix and with precoder that uses an equivalent DL MU-MIMO channel matrix is carried out in this paper. We also verify that using degrees of freedom to cancel the MU interference at RX become the system performance less susceptible to the negative effects of delay and compression in the CSI feedback.

III. Downlink MU-MIMO: Transceiver Design

A. *Received Signal Model For DL MU-MIMO Channel*

The received symbols in the frequency domain for the DL MU-MIMO OFDM channel with *K* users can be modeled as follows:

$$\boldsymbol{y} = \begin{bmatrix} y_1 \\ y_2 \\ \vdots \\ y_K \end{bmatrix} = \boldsymbol{H_{DL}}\boldsymbol{x} + \boldsymbol{z} = \begin{bmatrix} \boldsymbol{H}_1 \\ \boldsymbol{H}_2 \\ \vdots \\ \boldsymbol{H}_K \end{bmatrix} \cdot \left[x_1 x_2 \cdots x_{n_{ss,total}}\right]^T + \begin{bmatrix} z_1 \\ z_2 \\ \vdots \\ z_K \end{bmatrix}, \quad (1)$$

where the DL MU-MIMO channel is given by the matrix $\mathbf{H_{DL}}$ with size $n_{r,total} = \sum_{u=1}^{K} n_{r,u}$ by n_t, where $n_{r,u}$ is the number of receive antennas of the uth station (STA) and n_t is the number of transmit antennas at the access point (AP). The matrix $\mathbf{H_u}$, with size $n_{r,u}$ by n_t, models the DL MIMO channel matrix observed by the uth user [8, pp. 401].

The column vector $\mathbf{z}$ in (1) models the zero mean circular symmetric complex Gaussian (ZMCSCG) noise. This vector is formed by K random vectors, where each column vector $\boldsymbol{z}_u = \left[z_{u,1}, z_{u,2}, \cdots z_{u,n_{ru}}\right]^T, u = 1, \cdots K$, is composed by $z_{u,j}$ $(j = 1, .. n_{r,u})$ independent and identical distributed (i.i.d) ZMCSCG random variables (r.v.) with equal variance N_0.

The received signal by the uth user is given by

$$\boldsymbol{y_u} = \boldsymbol{H_u x} + \boldsymbol{z_u}, \quad \mathrm{u} = 1, \cdots \mathrm{K}. \quad (2)$$

The symbols at the output of the transmit antenna elements are given by $\boldsymbol{x} = \boldsymbol{P} \cdot \boldsymbol{s}$, where $\mathbf{P}$ is the pre-coding matrix with size n_t by $n_{ss,total} = \sum_{u=1}^{K} n_{ss,u}$, where $n_{ss,u}$ and $n_{ss,total}$ denote, respectively, the number of SS transmitted to the uth STA and the total number of SS transmitted to all K STAs. The transmitted symbols for all K users are modeled by the column vector $\mathbf{s} = \left[\mathbf{s}_{u,1}^T, \mathbf{s}_{u,2}^T, \cdots \mathbf{s}_{u,K}^T\right]^T$, where the symbols transmitted to the uth STA are given by the column vector $\boldsymbol{s_u} = \left[s_{u,1}, s_{u,2}, \cdots, s_{u,n_{ss,u}}\right]^T$. The DL transmitted symbol to the uth user at jth SS is denoted by $s_{u,j}$.

B. IEEE 802.11ac Channel Sounding Mechanism

The implementation of single user (SU) MIMO adaptive transmit beamforming (TxBF) and DL MU-MIMO in IEEE 802.11ac systems needs mechanisms to sound the channel in order to obtain the CSI at TX side. The 802.11ac amendment specifies only one sounding mechanism, which it is based on the transmission of non-data-packet (NDP) by the beamformer, as shown in Fig. 1 [2, pp. 438]. The beamformees feedback the CSI using the *Compressed Beamforming Frame (CBF)*.

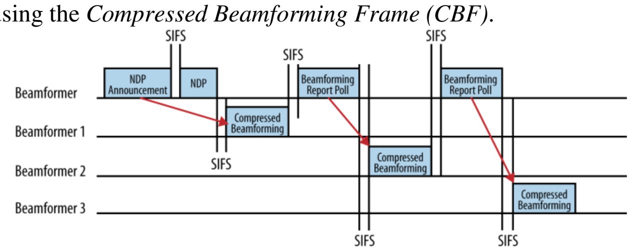

Figure 1. MU-MIMO sounding scheme used in 802.11ac. SIFS means Short InterFrame Spacing.

The explicit compressed feedback scheme specified in the 802.11ac amendment is based on the singular value decomposition (SVD) of the MIMO channel matrix observed at each STA involved in the sounding procedure, i.e.,

$$\boldsymbol{H}_u = \boldsymbol{U_u}\,\mathbf{S_u}\mathbf{V_u^H} = \boldsymbol{U_u}\left[\mathbf{S_u^{non-zero}}\mathbf{0}\right]\begin{bmatrix} (\mathbf{V_u^{non-zero}})^{\mathbf{H}} \\ (\mathbf{V_u^{zero}})^{\mathbf{H}} \end{bmatrix}. \quad (3)$$

Notice that the matrix $\mathbf{H_u}$ feed backed during the sounding procedure has size $n_{ss,u}$ by n_t, i.e., the rank depends on the user selection scheduling algorithm that specifies the channel dimensionality to be sounded. However, notice that during the phase of data transmission, the channel matrix has size $n_{r,u}$ by n_t, since all RX antennas must be used in the MIMO detection to improve the system performance.

The matrix $\boldsymbol{U_u} \in \mathbb{C}^{n_{ss,u} \times n_{ss,u}}$ has the left singular vectors of matrix $\boldsymbol{H}_u$. The matrix of singular values of $\boldsymbol{H}_u$ is denoted by $\mathbf{S_u} \in \mathbb{C}^{n_{ss,u} \times n_t}$, where the matrix that contains only the non-zero singular values is denoted by $\mathbf{S_u^{non-zero}} \in \mathbb{C}^{n_{ss,u} \times n_{ss,u}}$. The superscript $(.)^{\mathrm{H}}$ denotes Hermitian transpose operator.

The matrix $\boldsymbol{V_u} \in \mathbb{C}^{n_t \times n_t}$ is formed by the right singular vectors of the matrix $\boldsymbol{H}_u$. The matrices $\mathbf{V_u^{non-zero}} \in \mathbb{C}^{n_t \times n_{ss,u}}$ and $\widetilde{\mathbf{V}}_{\mathbf{u}}^{\mathbf{zero}} \in \mathbb{C}^{n_t \times (n_t - n_{ss,u})}$ contain the right singular vectors that correspond to the non-zero and zero singular values, respectively, of the matrix $\boldsymbol{H}_u$. $\mathbf{V_u^{zero}}$ is an orthonormal basis for the null space of $\boldsymbol{H_u}$.

The IEEE 802.11ac amendment specifies that each user involved in the sounding procedure must implement an algorithm based on Givens Rotation to compress the $\mathbf{V_u^{non-zero}}$ matrix in the form of two sets of angles. This information is transmitted in the *Compressed Beamforming Report field* of the *CBF*, as described in the next subsection.

In the MU-MIMO case, the *CBF* also contains the *MU Exclusive Beamforming Report* field, where the average signal-to-noise ratio ($\overline{\mathrm{SNR}}$) per SS and $SNR_{i,k}$ of the kth subcarrier (SC) at the ith SS are transmitted. The proprietary MIMO channel estimation scheme implemented at 802.11ac RX must use the pilots of the very-high throughput long training filed (VHT-LTF) transmitted in the preamble of NDP and data packets [2, pp. 195]. Since the cover matrix used to transmit the pilots in the VHT-LTF is orthogonal, then the average SNR can be estimated using classical techniques designed for OFDM systems [9]. Note that the average SNR is practically the same for each SS. The $SNR_{i,k}$, assuming that the transceiver implements a precoder based on SVD and MMSE MIMO detector, is given by [2, pp. 371]

$$SNR_{i,k} = \frac{1/\mathrm{n_t}}{\mathrm{N_0}} \frac{1}{\mathrm{diag_i}\left[(\boldsymbol{H}_u\mathbf{V_u^{non-zero}})^{\mathrm{H}}\,\boldsymbol{H}_u\mathbf{V_u^{non-zero}}\right]}$$

$$SNR_{i,k} = \overline{\mathrm{SNR}} \cdot \mathrm{S_{i,k}^2}, \quad (4)$$

where it is assumed the transmitted power is normalized.

Finally, the beamformer can built the channel equivalent matrix using the information transported by the CABF (i.e., compressed $\mathbf{V_u^{non-zero}}$, $\overline{\mathrm{SNR}}$ and $SNR_{i,k}$), i.e.,

$$\boldsymbol{H_{EQ}} = \begin{bmatrix} \mathbf{S_1^{non-zero}}(\mathbf{V_1^{non-zero}})^{\mathbf{H}} \\ \mathbf{S_2^{non-zero}}(\mathbf{V_2^{non-zero}})^{\mathbf{H}} \\ \vdots \\ \mathbf{S_K^{non-zero}}(\mathbf{V_K^{non-zero}})^{\mathbf{H}} \end{bmatrix}. \quad (5)$$

The above matrix is the one effectively used at the TX to calculate the precoding matrix when the technical details of the IEEE 802.11ac sounding procedure are taken into account, i.e., the real-world scenario. Note that the matrix $\mathbf{U_u}$ is not present in (5). However, the information contained in this matrix is incorporated in the effective MIMO channel matrix estimated by the uth STA, which it is necessary to calculate the MIMO detector. Observe that the VHT-LTF are precoded by the matrix $\mathbf{P}$ when the medium access control packet data units (MPDU) are transmitted from the beamformer to the beamformees.

C. 802.11AC COMPRESSION: GIVENS PLANAR ROTATION

The use of Givens rotation allows representing unitary matrices using angles of polar coordinates, and, consequently, the number of bits necessary to represent unitary matrices can be compressed. The unitary matrix $\mathbf{V}_{\mathbf{u}}^{\mathbf{non-zero}}$ originated from applying SVD in MIMO channel matrix observed by the uth STA is given by (6), where $\tilde{\boldsymbol{I}}_{n_t \times n_{r_u}}$ is an modified unitary matrix with size $n_t \times n_{ss_u}$ with extra rows or columns composed with zeros when $n_t \neq n_{ss_u}$.

$$\mathbf{V}_{\mathbf{u}}^{\mathbf{non-zero}} = \left(\prod_{i=1}^{min(n_t,n_{r_u})} \left[\boldsymbol{D}_i \prod_{j=i+1}^{n_t} \boldsymbol{G}_{ji}^T\left(\boldsymbol{\psi}_{j,i}\right)\right] \times \tilde{\boldsymbol{I}}_{n_t \times n_{ss_u}}\right) \tilde{\boldsymbol{D}} \text{ . } \quad (6)$$

The Givens planar rotation operates over real numbers, but the unitary matrix $\mathbf{V}_{\mathbf{u}}^{\mathbf{non-zero}}$ belongs to the complex field. Therefore, it is necessary to use the matrices $\boldsymbol{D}_i$ and $\tilde{\boldsymbol{D}}$ as follows: the diagonal matrix $\tilde{\boldsymbol{D}}$ with size $n_{ss_u} \times n_{ss_u}$ has its main diagonal elements given by $\{e^{j\theta_i}, i = 1, \cdots, n_{ss_u}\}$, such as the last row of the matrix $\mathbf{V}_{\mathbf{u}}^{\mathbf{non-zero}} \tilde{\boldsymbol{D}}^{\boldsymbol{H}}$ contains only non-negative real values. These angles are given by $\theta_i = angle(\ \mathbf{V}_{\mathbf{u}}^{\mathbf{non-zero}})$.

The diagonal matrix $\boldsymbol{D}_i$ is given by

$$\boldsymbol{D}_i = \begin{bmatrix} \boldsymbol{I}_{i-1} & 0 & \cdots & \cdots & 0 \\ 0 & e^{j\phi_{i,i}} & 0 & \cdots & 0 \\ \vdots & 0 & \ddots & 0 & \vdots \\ \vdots & \vdots & 0 & e^{j\phi_{n_t,i}} & 0 \\ 0 & 0 & \cdots & 0 & 1 \end{bmatrix}, \quad (7)$$

where the angles $\{\phi_{j,i}, j = 1, \cdots, n_t - 1; i = 1, \cdots, n_t\}$ are obtained such as all elements of ith column of $\boldsymbol{D}_i^{\boldsymbol{H}}(\ \mathbf{V}_{\mathbf{u}}^{\mathbf{non-zero}} \tilde{\boldsymbol{D}}^{\boldsymbol{H}})$ are all non-negative real numbers, i.e., $\phi_{j,i} = angle(\ \mathbf{V}_{\mathbf{j,i}}^{\mathbf{non-zero}})$. Observe that the matrix $\boldsymbol{D}_i^{\boldsymbol{H}}$ does not change the last row of matrix $\mathbf{V}_{\mathbf{u}}^{\mathbf{non-zero}}$ since the last element of its diagonal principal is one. Therefore, this is the reasoning why the matrix $\mathbf{V}_{\mathbf{u}}^{\mathbf{non-zero}}$ must be right-multiplied by the matrix $\tilde{\boldsymbol{D}}^{\boldsymbol{H}}$, as earlier described.

The Givens matrix is given by (8), where $\mathbf{I}_{\mathbf{n}}$ denotes the identity matrix with size n and the term $cos(\psi_{j,i})$ is located at jth row and ith column.

$$\boldsymbol{G}_{ji}(\boldsymbol{\psi}) = \begin{bmatrix} \boldsymbol{I}_{i-1} & 0 & 0 & 0 & 0 \\ 0 & cos(\psi_{j,i}) & 0 & sin(\psi_{j,i}) & 0 \\ 0 & 0 & \boldsymbol{I}_{j-i-1} & 0 & 0 \\ 0 & -sin(\psi_{j,i}) & 0 & cos(\psi_{j,i}) & 0 \\ 0 & 0 & 0 & 0 & \boldsymbol{I}_{n_t-1} \end{bmatrix}. \quad (8)$$

The coefficients of each Given matrix are obtained by solving the following problem [2, pp. 388]

$$\begin{bmatrix} cos(\psi) & sin(\psi) \\ -sin(\psi) & cos(\psi) \end{bmatrix} \begin{bmatrix} x_1 \\ x_2 \end{bmatrix} = \begin{bmatrix} \mathrm{y} \\ 0 \end{bmatrix} = \begin{bmatrix} \sqrt{\mathrm{x}_1^2 + \mathrm{x}_2^2} \\ 0 \end{bmatrix}, \quad (9)$$

where x_1 e x_2 denote the *real values* from the matrix where the planar rotation is being performed. The solution of (9) is given by

$$\psi = cos^{-1}\left(\frac{x_1}{\sqrt{\mathrm{x}_1^2+\mathrm{x}_2^2}}\right) = sin^{-1}\left(\frac{x_2}{\sqrt{\mathrm{x}_1^2+\mathrm{x}_2^2}}\right), \quad (10)$$

The set of angles that must be feedback to obtain the matrix $\mathbf{V}_{\mathbf{u}}^{\mathbf{non-zero}}$ from (6) are given in [1]. For example, for a typical configuration with four transmit antennas and two receive antennas, each STA must feedback the following angles:

$$\{\phi_{1,1}, \phi_{2,1}, \phi_{3,1}, \psi_{2,1}, \psi_{3,1}, \psi_{4,1}, \phi_{2,2}, \phi_{3,2}, \psi_{3,2}, \psi_{4,2}, \phi_{3,3}, \psi_{4,3}\}, \quad (11)$$

Observe that the angles $\{\theta_i, i = 1, \cdots, n_{r_u}\}$ used to built the matrix $\tilde{\boldsymbol{D}}$ are not feedback. Hence, the TX only can rebuilt the matrix $\mathbf{V}_{\mathbf{u}}^{\mathbf{non-zero}} \tilde{\boldsymbol{D}}^{\boldsymbol{H}}$. However, using this approximate matrix does not change the observable SNR at RX side [2, pp. 389].

The angles ϕ and ψ are quantized in the ranges $[0,2\pi)$ and $[0,\pi/2)$, respectively, as follows:

$$\begin{cases} \phi = \frac{k\pi}{2^{b+1}} + \frac{\pi}{2^{b+2}}, & k = 0, \cdots, 2^{b+2} - 1 \\ \psi = \frac{k\pi}{2^{b+2}} + \frac{\pi}{2^{b+2}}, & k = 0, \cdots, 2^b - 1 \end{cases}, \quad (12)$$

where *(b+2)* and *(b)* are number of bits to quantize the angles ϕ and ψ, respectively. Note that *(b)* can be *1,2,3* or *4*.

D. MU-MIMO PRECODING

The regularized channel inversion minimum mean squared error (RI-MMSE) precoding matrix, considering that all STAs have the same average SNR, is given by [10]

$$\boldsymbol{P}_{\boldsymbol{MMSE}} = \beta_{\mathrm{MMSE}} \cdot \boldsymbol{H}_{\boldsymbol{DL}}^{\boldsymbol{H}} \cdot \left[\boldsymbol{H}_{\boldsymbol{DL}} \cdot \boldsymbol{H}_{\boldsymbol{DL}}^{\boldsymbol{H}} + \frac{1}{\mathrm{SNR}} \mathbf{I}_{n_{ss,total}}\right]^{-1}, \quad (13)$$

where $\mathbf{I}_{n_{ss,total}}$ denotes a diagonal matrix with dimension $n_{ss,total}$ and the normalization factor of the transmitted power is given by

$$\beta_{MMSE} = \sqrt{\frac{\mathrm{n_t}}{\mathrm{trace}(\boldsymbol{P}_{\boldsymbol{MMSE}} \cdot \boldsymbol{P}_{\boldsymbol{MMSE}}^{\boldsymbol{H}})}}. \quad (14)$$

The feedback scheme specified in the 802.11ac amendment, as earlier described, does not allow that the TX rebuilt the MU-MIMO channel matrix $\mathbf{H}_{\mathbf{u}}$ for each one of the K users. Therefore, the equivalent channel matrix $\mathbf{H}_{\mathbf{EQ}}$ given by (5) must replace $\mathbf{H}_{\mathbf{DL}}$ in (13) when the real world concerns are in vogue.

E. MMSE AND IC-MMSE MU-MIMO DETECTORS

The received signal vector at the output of the MIMO detector for the uth STA can be modeled as

$$\tilde{\boldsymbol{y}}_{\boldsymbol{u}} = \boldsymbol{W}_{\boldsymbol{u}}^{\boldsymbol{H}} \boldsymbol{y}_{\boldsymbol{u}} = \boldsymbol{W}_{\boldsymbol{u}}^{\boldsymbol{H}} \cdot (\boldsymbol{H}_{\boldsymbol{u}} \boldsymbol{P} \boldsymbol{s} + \boldsymbol{z}_{\boldsymbol{u}}), \quad (15)$$

where the received signal for the uth STA is given by (2) and the matrix $\mathbf{W}_{\mathbf{u}}$, with size size $n_{r,u}$ by $n_{ss,u}$, denotes the linear MIMO detector for the uth STA.

Eq. (15) can be rewritten as

$$\tilde{\boldsymbol{y}}_{\boldsymbol{u}} = \boldsymbol{W}_{\boldsymbol{u}}^{\boldsymbol{H}} \cdot (\boldsymbol{H}_{\boldsymbol{u}} \boldsymbol{P}_{\boldsymbol{1}} \boldsymbol{s}_{\boldsymbol{1}} + \cdots + \boldsymbol{H}_{\boldsymbol{u}} \boldsymbol{P}_{\boldsymbol{u}} \boldsymbol{s}_{\boldsymbol{u}} + \cdots + \boldsymbol{H}_{\boldsymbol{u}} \boldsymbol{P}_{\boldsymbol{K}} \boldsymbol{s}_{\boldsymbol{K}} + \boldsymbol{z}_{\boldsymbol{u}}), \quad (16)$$

where $\mathbf{P}_{\mathbf{u}}$, with dimension n_t by $n_{ss,u}$, denotes the columns of the matrix $\mathbf{P}$ used to precoding the symbols transmitted to the uth STA. Denoting the effective channel matrix observed by uth user as $\tilde{\boldsymbol{H}}_{\boldsymbol{u}} = \boldsymbol{H}_{\boldsymbol{u}} \boldsymbol{P}$, i.e.,

$$\tilde{\boldsymbol{H}}_{\boldsymbol{u}} = [\boldsymbol{H}_{\boldsymbol{u}} \boldsymbol{P}_{\boldsymbol{1}}, \cdots \boldsymbol{H}_{\boldsymbol{u}} \boldsymbol{P}_{\boldsymbol{u}}, \cdots, \boldsymbol{H}_{\boldsymbol{u}} \boldsymbol{P}_{\boldsymbol{K}}] = [\tilde{\boldsymbol{H}}_{\boldsymbol{u},\boldsymbol{1}}, \cdots \tilde{\boldsymbol{H}}_{\boldsymbol{u},\boldsymbol{u}}, \cdots, \tilde{\boldsymbol{H}}_{\boldsymbol{u},\boldsymbol{k}}]. \quad (17)$$

then (15) and (16) can be conveniently rewritten as (18) and (19), respectively.

$$\tilde{\boldsymbol{y}}_{\boldsymbol{u}} = \boldsymbol{W}_{\boldsymbol{u}}^{\boldsymbol{H}} \cdot (\tilde{\boldsymbol{H}}_{\boldsymbol{u}} \boldsymbol{s} + \boldsymbol{z}_{\boldsymbol{u}}). \quad (18)$$

$$\tilde{\boldsymbol{y}}_{\boldsymbol{u}} = \boldsymbol{W}_{\boldsymbol{u}}^{\boldsymbol{H}} \cdot (\tilde{\boldsymbol{H}}_{\boldsymbol{u},\boldsymbol{1}} \boldsymbol{s}_{\boldsymbol{1}} + \cdots + \tilde{\boldsymbol{H}}_{\boldsymbol{u},\boldsymbol{u}} \boldsymbol{s}_{\boldsymbol{u}} + \cdots + \tilde{\boldsymbol{H}}_{\boldsymbol{u},\boldsymbol{K}} \boldsymbol{s}_{\boldsymbol{K}} + \boldsymbol{z}_{\boldsymbol{u}}), \quad (19)$$

If the MU interference is perfectly cancelled by the precoder, then (19) can be modified to

$$\tilde{\boldsymbol{y}}_{\boldsymbol{u}} = \boldsymbol{W}_{\boldsymbol{u}}^{\boldsymbol{H}} \cdot (\tilde{\boldsymbol{H}}_{\boldsymbol{u},\boldsymbol{u}} \boldsymbol{s}_{\boldsymbol{u}} + \boldsymbol{z}_{\boldsymbol{u}}). \quad (20)$$

Therefore, using (20), the MMSE MIMO detector to the uth user is given by

$$\boldsymbol{W}_{\boldsymbol{MMSE},\boldsymbol{u}} = \left[\tilde{\boldsymbol{H}}_{\boldsymbol{u},\boldsymbol{u}} (\tilde{\boldsymbol{H}}_{\boldsymbol{u},\boldsymbol{u}})^{\boldsymbol{H}} + \frac{I_{n_{r,u}}}{SNR_u}\right]^{-1} \cdot \tilde{\boldsymbol{H}}_{\boldsymbol{u},\boldsymbol{u}}. \quad (21)$$

However, if the cancellation of MU interference is imperfect, the MMSE MIMO detector, using (19), is given by [11]

$$\boldsymbol{W_{MMSE,u}} = \left[\widetilde{\boldsymbol{H}}_{\boldsymbol{u}}(\widetilde{\boldsymbol{H}}_{\boldsymbol{u}})^{\boldsymbol{H}} + \frac{\boldsymbol{I_{n_{r,u}}}}{SNR_u}\right]^{-1} \cdot \widetilde{\boldsymbol{H}}_{\boldsymbol{u,u}}. \qquad (22)$$

Henceforth, we label the linear detectors that implement (22) as follows: *(1)* the interference cancellation MMSE (IC-MMSE) MIMO detector has more receive antennas than the number of SS transmitted to the *u*th STA (i.e., spatial degrees of freedom are used to improve the cancelling of MU-MIMO interference); *(2)* the MSSE MIMO detector has an equal number of receive antennas and SS transmitted to the *u*th STA. Finally, note that (22) resumes to (21) for single-user (SU) MMSE MIMO detector.

III. Performance Analyzes

Tab. I shows the main characteristics of the IEEE 802.11ac simulator that we have been developing [12]. In this paper, we use a BW of 80 MHz and soft-decision Viterbi decoding. Tab. II shows the 802.11ac modulation code schemes (MCS) analyzed in this paper.

Table I– Parameters of IEEE 802.11ac simulator [12].

Parameter	Value	Parameter	Value
Carrier Frequency	5.25 GHz	MCS	0-9
Bandwidth	20 MHz, 40 MHz, 80 MHz	Number of Spatial Streams	1 to 8
GI Length	800 ns	Synchronization	Auto-Correlation
Modulation	BPSK, QPSK, 16-QAM, 64QAM, 256-QAM	MIMO Channel Estimation	Least Square
Binary Convolutional Code (BCC)	Code rate: r=1/2, r=2/3, r=3/4, r=5/6	Channel Decoder	Hard and Soft-Decision Viterbi Decoding

Table II - MCS investigated in this paper. The PHY data rates assume a guard-interval (GI) of 800 ns and BW of 80 MHz.

	Mod	BCC Code Rate	# SSs	Data Rate Mbps
0	BPSK	1/2	1	29.3
			2	58.5
1	QPSK	1/2	1	58.5
			2	117.0
2	QPSK	3/4	1	87.8
			2	175.5
3	16-QAM	1/2	1	117.0
			2	234.0

In the sequel, MU-MIMO TGac channels with n_t transmit antennas, an equal number of $n_{r,u}$ receive antennas per each one of the K STAS that load the channel is denoted by *TGac* [n_t,n_r,*K*,n_{ss}], where the same number of SS, n_{ss}, is transmitted for each one of the K STAs. The simulation results assume the spatial correlated and frequency selective TGac D channel model [13]: a typical office channel with maximum excess delay of *390 ns* and root mean square (rms) delay spread of *50 ns* [2, pp. 38]. The Doppler power spectrum (DPS) in TGn MIMO channel model is modeled by [2, pp. 45]

$$S_d(f) = \frac{\sqrt{A}/(\pi f_d)}{1+A\left(\frac{f}{f_d}\right)}, \quad |f| \leq f_{max}, \qquad (23)$$

where $\boldsymbol{f_d} = \frac{v}{c}\boldsymbol{f_c}$ denotes the Doppler spread; f_c denotes the carrier frequency in Hz; *c* the speed of light and v_0 is the environmental speed (i.e., v_0 is fixed in *1.2 km/h*, given $f_d \cong 6\,Hz\ at\ 5\ GHz\ band$ and coherence time of *50 ms* when correlation of *50%* is assumed). The *constant A* equal to *9* means that the spectrum is *10 dB* below the peak at the Doppler spread frequency.

The *system default configuration* assumes no compression of the feedback; no Doppler and MPDU payload of *1500 octets*.

A. Effect of Equivalent Channel Matrix on the Transceiver Performance

Fig. 2 compares the performance of 802.11ac transceiver with RI-MMSE precoder that uses either the *"complete"* $\mathbf{H_{DL}}$ channel matrix or the equivalent DL MU-MIMO channel matrix given by (5). The RX implements the MMSE MIMO detector. This figure shows the MPDU packet error rate (PER) as a function of SNR over the *TGac D [4,2,2,2]* channel. Surprisingly, for MCS0 and MCS1, the performance of RI-MMSE precoder that uses the equivalent DL MU-MIMO channel matrix $\mathbf{H_{EQ}}$ presents a superior performance w.r.t. the RI-MMSE precoder that uses the *"complete"* $\mathbf{H_{DL}}$ matrix (see Eq. 1). This happens because the noise increases the entropy in the CSI when the matrix of left-singular vector is included in the feedback. However, the same performance is observed for MCS3 for both types of CSI feedback since the higher SNR decreases the noise effects in the estimated CSI.

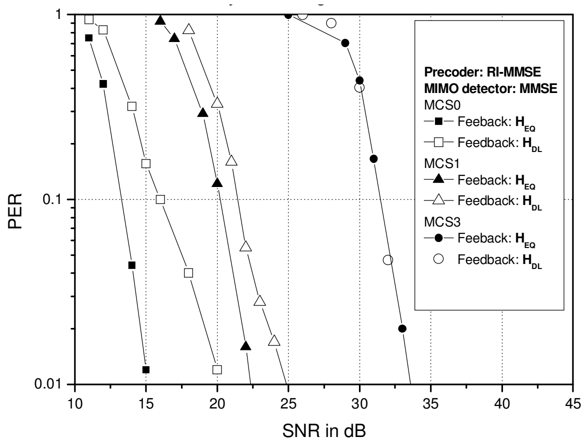

Figure 2. Effects on the PER of the CSI used to calculate the RI-MMSE precoder: *TGac D [4,2,2,2]* MIMO channel and MMSE MIMO detector.

- **Lesson 1:** *the feedback specified in the IEEE 802.11ac amendment improves the performance at medium SNR regime in relation to systems that use the complete DL MU-MIMO channel matrix in the precoding calculation when the MMSE MIMO detector is implemented.*

Fig. 3 shows that the same performance is obtained when the RI-MMSE precoder uses either the matrix $\mathbf{H_{DL}}$ or the matrix $\mathbf{H_{EQ}}$ to calculate the matrix $\mathbf{P_{MMSE}}$ when the receiver implements the IC-MMSE MIMO detector over the TGac D [4,2,4,1] MIMO channel. Finally, note that this figure also depicts a severe performance degradation when the TX uses only the matrix $\mathbf{V}$ to calculate the RI-MMSE precoder for both configurations used at RX side, i.e., IC-MMSE and MMSE MIMO detectors.

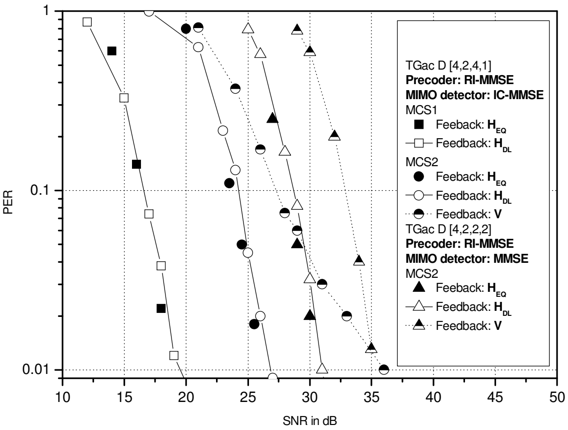

Figure 3. Effects on the PER of the CSI used to calculate the RI-MMSE precoder: *TGac D [4,2,4,1]* MIMO channel with IC-MMSE MIMO detector and *TGac D [4,2,2,2]* MIMO channel and MMSE MIMO detector.

- ***Lesson 2:*** *the implementation of IC-MMSE MIMO detector at RX side decreases the power loss sensibility w.r.t the type of CSI (H_{DL} or H_{Eq}) feed backed by the beenformees.*
- ***Lesson 3:*** *the precoder should use the matrix of singular values to built the equivalent channel matrix in order to avoid detrimental performance degradation.*

B. Effect of Feedback Compression on the Transceiver Performance

Figures 4 and 5 investigate the effects of compressed feedback on the performance of MU-MIMO transceivers with RI-MMSE precoder and, respectively, MMSE (TGac D [4,2,2,2]) and IC-MMSE (TGac D [4,2,4,1]) MIMO detectors. Note that the number of bits necessary to avoid power losses has a strong dependence with the MIMO detector implemented and MCS used. For example, a system with MMSE MIMO detector (see Fig. 4) needs to set *b* in (12) to 3 , i.e. $(\boldsymbol{\psi},\boldsymbol{\phi})=(\mathbf{3},\mathbf{5})\ \boldsymbol{bits}$; and b=5 , i.e. $(\boldsymbol{\psi},\boldsymbol{\phi})=(\mathbf{5},\mathbf{7})$ bits, for MCS0 and MCS3, respectively. However, only *b=1*, i.e., $(\boldsymbol{\psi},\boldsymbol{\phi})=(\mathbf{5},\mathbf{7})$ bits are necessary for MCS0 when IC-MMSE MIMO detector is implemented, as shown in Fig. 6.

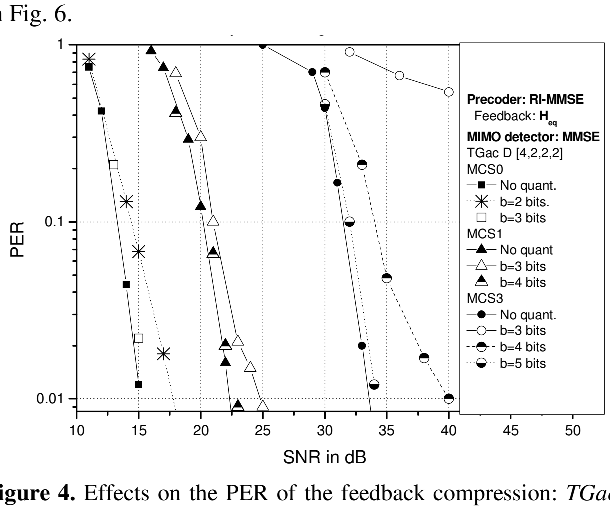

Figure 4. Effects on the PER of the feedback compression: *TGac D [4,2,2,2]* MIMO channel with MMSE MIMO detector.

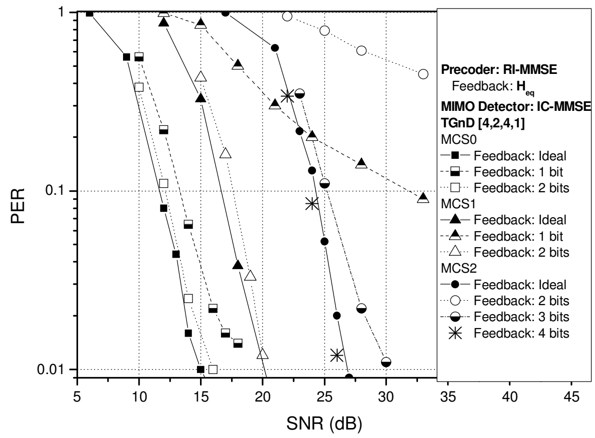

Figure 5. Effects on the PER of the feedback compression *TGac D [4,2,4,1]* MIMO channel with IC-MMSE MIMO detector.

- ***Lesson 4:*** *transceivers with IC-MMSE MIMO detector present lower sensibility with feedback compression w.r.t. transceivers that implement MMSE MIMO detectors.*
- ***Lesson 5:*** *the number of bits necessary to compress the information without power losses should be determined on the flight using smart iterative algorithms since the system performance presents a strong dependence with a multitude of variables (e.g., MIMO detector, MCS, channel characteristics).*

C. Effect of Doppler Spread on the Transceiver Performance

Fig. 6 allows inferring conclusions on the joint effects of feedback compression and delay on the PER for the following configurations: *TGac D [4,2,2,2]* MIMO channel with MMSE MIMO detector and *TGac D [4,2,4,1]* MIMO channel with IC-MMSE MIMO detector.

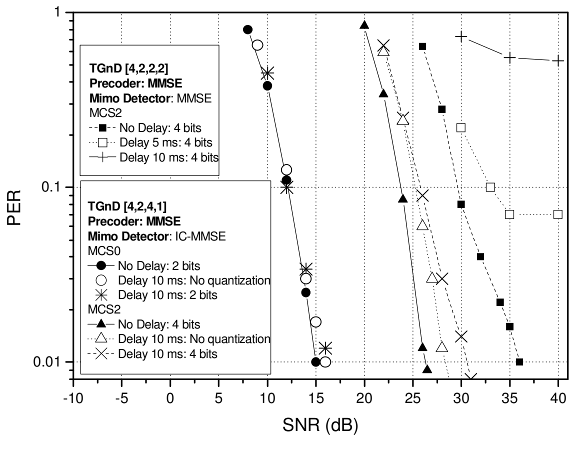

Figure 6. Effects on the PER of the feedback compression and delay on the PER: *TGac D [4,2,2,2]* MIMO channel with MMSE MIMO detector and *TGac D [4,2,4,1]* MIMO channel with IC-MMSE MIMO detector.

- ***Lesson 6:*** transceivers with IC-MMSE MIMO detector present significant lesser dependence w.r.t channel sounding delay than the MMSE MIMO detector.
- ***Lesson 7:*** the joint effects of feedback delay and compression on the performance of IC-MMSE MIMO detector presents a dependence with the MCS (e.g., no power loss for MCS0 and *2.5 dB* power loss for MCS2).

IV. CONCLUSIONS

First, we described related contributions in the field of transceiver design for the DL in MU-MIMO 802.11ac WLANs, emphasizing our main contribution, i.e., a performance evaluation of RI-MMSE precoder and IC-MMSE MIMO detector with compressed feedback over TGac MIMO channels with Doppler spread. Then, we presented a derivation of the IC-MMSE MIMO detector and the IEEE 802.11ac simulator characteristics. After having established a common background, we showed a unified set of simulation results and lessons learned on the effects of CSI feedback compression and delay upon the 802.11ac DL MU-MIMO performance. Finally, we have concluded that the effects of realistic system configuration on the performance of DL MU-MIMO transceivers depend strongly on a multitude of parameters and assumptions (channel model, number of quantization bits, MIMO detectors scheme and so forth). Therefore, we claim that the developing of real time radio resource algorithms is a fundamental issue to set up on the flight the system configuration in order to balance accordingly the tradeoff between user satisfaction and system complexity.

In the full version of this paper, we shall analyze the comparatively effects of compressed feedback delay on the performance on single-user (SU) transmit beamforming (TxBF) and MU-MIMO transceivers. We also show results on performance of MU-MIMO schemes with MIMO detectors based on lattice reduction (LR) techniques.

REFERENCES

[1] Wireless LAN Medium Access Control and Physical Layer Specifications, Amendment 5: Enhancement for Very High Throughput for Operations in Bands below 6 GHz. IEEE P802.11ac, Dec., 2013.

[2] E. Perahia and R. Stacey, *Next Generation Wireless LANS*: *802.11n and 802.11ac.2th ed*. Cambridge: Cambridge University Press, 2013.

[3] VK Jones and H. Sampath. "Emerging technologies for WLAN," in *IEEE Communication Magazine,* vol. 53, no. 3, pp. 141-149, March, 2015.

[4] M. Kim and J. Kim. "Adaptive interference-aware receiver for multi-user MIMO downlink in IEEE 802.11ac," *in 2015 IEEE International Conference on Consumer Electronics (ICCE)*, pp. 645-646, Las Vegas, 2015.

[5] H. Lou, M. Ghosh, P. Xia and R. Olesen. "A comparison of implicit and explicit channel feedback methods for MU-MINO WLAN systems, " in 2013 IEEE 24th International Symposium on Personal, Indoor and Mobile Radio Communication Systems (PIRMC 2013), pp. 419-424, London, 2014.

[6] W. Lin et. al. "Performance of linear precoding and user selection in IEEE 802.11ac downlink MU-MIMO system," in *2014 IEEE Wireless Communications and Networking Conference (WCNC),* Istanbul, 2014.

[7] J. Park et. al. "A high performance MIMO detection algorithm for DL MU-MIMO with practical errors in IEEE 802.11ac systems," in *2013 IEEE 24th Symp. on Personnal, Indoor and Moobile Radio Communications,* 2013.

[8] Y. S. Cho, J. Kim, W. Y. Yang and C. G. Kang, *MIMO-OFDM Wireless Communications with MATLAB*. Singapore: John Wiley & Sons, 2010.

[9] R. S. Manzoor et al. "Front-end estimation of noise power and SNR in OFDM systems, "*in International Conference on Intelligent and Advanced Systems 2007 (ICIAS 2007),* Kuala Lumpur, 2007.

[10] C. B Peel, B. M. Howhwald and A. L. Swindlehurst. "A vector - pertubation technique for near-capacity multi antenna multiuser communication - Part I: channel inversion and regularization," in *IEEE Transactions on Communications*, vol. 53, no. 1, pp. 195-202, Feb. 2005.

[11] S. Veramani and A. V. Zelst, *Interference cancellation for downlink MU-MIMO*. IEEE 802.11-09/1234r1, 2010.

[12] R. P. F. Hoefel. "Multi-User OFDM MIMO in IEEE 802.11ac WLAN: a simulation framework to analysis and synthesis", in *IEEE Latin America Transactions,* vol.13, no. 2, pp.540-545, Feb., 2015.

[13] G. Breit, H. Sampath, S. Vermani, et. al., *TGac Channel Model Addendum Support Material.* IEEE 802.11-09/06/0569r0, May, 2009.